Giant magnetoresistive thin films of $(La,Pr)_{0.7}(Ca,Sr)_{0.3}MnO_3$ prepared by aerosol MOCVD

O. Yu. Gorbenko,*[a] A. R. Kaul,[a] N. A. Babushkina[b] and L. M. Belova,[b]

[a]*Chemistry Department, Moscow State University, 119899 Moscow, Russia*
[b]*Kurchatov Institute, 123182 Moscow, Russia*

It has been demonstrated that high quality thin films of $Ln_{1-x}M_xMnO_3$ can be successfully prepared by aerosol MOCVD at 750 °C from volatile thd complexes. Subsequent annealing in oxygen at 750 °C is necessary to stabilize the oxygen content of the films. XRD patterns of the films showed them to be pseudocubic with an apparent lattice parameter linear in the average ionic radius of Ln and M. The evolution of $Ln_{1-x}M_xMnO_3$ film morphology with increasing the film thickness has also been studied. The morphological instability of the MOCVD process results in the formation of a hillocky surface with thickness >2000 Å. The electrical properties of $La_{1-x}Ca_xMnO_3$ and $La_{1-x}Sr_xMnO_3$ correlate with those reported for bulk and thin film materials. The substitution of Pr for La in $La_{1-x}Sr_xMnO_3$ reduces the maximum resistivity temperature, T_p, non-linearly. $La_{1-x}Ca_xMnO_3$ thin films reveal a shift of T_p downwards in the case of substrate materials with a positive lattice mismatch with the films. $La_{0.35}Pr_{0.35}Ca_{0.3}MnO_3/LaAlO_3$ demonstrates a very complex temperature dependence of the resistivity, which is described using a conceptual phase diagram of $Ln_{1-x}M_xMnO_3$. A marked GMR effect was observed for $La_{0.35}Pr_{0.35}Ca_{0.3}MnO_3/LaAlO_3$ below 21 K (*ca.* 10^{10}%) and at *ca.* 70 K even in a field of 1 T.

$Ln_{1-x}M_xMnO_3$ perovskites, where Ln^{3+} is a rare-earth-metal cation and M is a doubly charged cation with a large ionic radius, with both Ln and M populating the A positions of the ABO_3 perovskite lattice, have attracted considerable attention owing to the recent discovery of giant negative magnetoresistance (GMR) of such compounds.[1] The GMR ratio $\rho = [R(0)-R(H)]/R(H)$, which can be easily reduced to $R(0)/R(H)$, where $R(0)$ and $R(H)$ represent the resistance in zero field and that in an applied magnetic field $H = 1$–10 T (irrespective of whether H is the saturation field or not), characterizes the effect. A variety of possible applications[2] such as sensors, reading heads, random access memory and hard disks with areal densities up to 10 Gbit in^{-2}, requires not only a large ρ but also a high sensitivity to the driving field $d\rho(H)/dH$ as well as a relatively low saturation field. The most widely studied perovskites, $La_{1-x}M_xMnO_3$,[3–9] leave much to be desired to satisfy these demands. That the role of the average ionic radii of the cations in the A positions (r_A) is crucial was recently explained.[4,10,11] By decreasing r_A, a higher ρ can be achieved. The nature of the substituting cation is also important. Changing the M cation to a cation with a smaller r_A shifts the temperature of the second-order phase transition (P→FMM) from a high-temperature paramagnetic phase (P) with activated conductivity to a low-temperature ferromagnetic phase with metal-like conductivity (FMM) downwards.[10,12] The variation of Ln has a similar but more complicated effect. A variety of new phase states appears for Ln = Pr or Nd.[13–16] Finally, the x range where a metal-like ferromagnetic phase exists is restricted to $0.2 < x < 0.5$ with a dome-shaped dependence of the magnetization on x.[17] Thus, it is reasonable to stay in the middle of this range in order to analyse the effect of Ln or M variation correctly.[10]

Comparable values of ρ were observed for both ceramics and thin films, causing us to reject the initial hypothesis which had connected high ρ values with thin epitaxial films.[18,19] Nevertheless, the electrophysical properties reported for films and bulk materials of practically the same composition can differ drastically (compare for instance ref. 10 and 20), and even the substrate material can influence the phase transitions in the manganite films.[21]

In the work reported here we prepared $Ln_{0.7}M_{0.3}MnO_3$ (Ln = La, Pr and M = Sr,Ca) thin films by aerosol MOCVD and studied their structures and electrical properties.

Experimental

Aerosol MOCVD, which was used to prepare the thin films, involves deposition from precursor vapours produced by the evaporation of their organic solutions nebulized in the carrier gas flow.[22,23] This method was found to combine reproducibility of vapour composition with flexibility of composition variation. Deposition conditions are summarized in Table 1. The $Ln_{0.7}M_{0.3}MnO_3$ thin films prepared are listed in Table 2. Volatile precursors were as follows: $La(thd)_3$, $Pr(thd)_3$, $Sr(thd)_2$, $Ca(thd)_2$ and $Mn(thd)_3$ (thd = 2,2,6,6-tetramethylheptane-3,5-dionate). All precursors were synthesized by standard techniques and sublimed in a vacuum before use.

Table 1 Parameters of the deposition process

parameter	value
stagnation flow reactor type	cold wall
deposition temperature/°C	750
total pressure/mbar	6
total gas flow/l h^{-1}	20
partial pressure of O_2/mbar	3
deposition rate/μm h^{-1}	0.5–1
solvent[a] consumption/ml h^{-1}	20
evaporator temperature/°C	250

[a]Diglyme ($CH_3OCH_2CH_2OCH_2CH_2OCH_3$) with 5 vol.% Hthd

Table 2 Thin films of $(La_{1-x},Pr_x)_{0.7}M_{0.3}MnO_3$ prepared in this work

M	x	abbreviation	substrates[a]
Sr	0	LSM	MgO, YSZ[b], $LaAlO_3$
Ca	0	LCM	MgO, YSZ, $LaAlO_3$, $SrTiO_3$
Sr	11xf.0	PSM	MgO, $LaAlO_3$
Ca	1	PCM	MgO, $LaAlO_3$
Sr	0.5	LPSM	MgO, $LaAlO_3$
Ca	0.5	LPCM	MgO, YSZ, $LaAlO_3$

[a]Substrate orientation (001) in the pseudocubic system. [b]YSZ = $ZrO_2(Y_2O_3)$

XRD [four-circle diffractometer, Siemens D5000 with secondary graphite monochromator (Cu-Kα radiation)] was applied to determine the phase composition, orientation and lattice parameters of the prepared films. θ–2θ, φ scans and rocking-curve measurements were used. SEM was accomplished by CAMSCAN equipped with an EDAX system for quantitive analysis. SNMS (sputtered neutrals mass spectrometry) depth profiling was carried out with an INA-3 system. Electrical resistivity measurements were carried out in a conventional four-point probe configuration using 3×10 mm^2 bars cut from the 10×10 mm^2 specimens.

Results and Discussion

Post-deposition treatment

Post-deposition annealing is known to influence the electrical properties of $Ln_{1-x}M_xMnO_3$.[5,19] For the preliminary experiments we prepared $La_{1-x}Sr_xMnO_{3+\delta}$ films with $x=0.15$ and 0.30.

As-grown films showed broad and sometimes split peaks of the perovskite phase in the XRD patterns (Fig. 1) with poorly reproducible lattice constants. It was suggested that such behaviour originated from incomplete oxidation at the cooling stage. Since the deposition was carried out at low oxygen partial pressure (Table 1), and an additional depletion was possible because of the consumption of oxygen to oxidize solvent molecules on the film surface, the as-grown film was expected to be reduced. The fact that after the deposition, reoxidation started but was incomplete under the cooling conditions, resulted in the XRD pattern observed.

The solution to the problem was found to consist of subsequent annealing of the films prepared by aerosol MOCVD in oxygen at 750 °C for 0.5 h. The choice of the annealing conditions was based on the data of van Roosmalen et al.,[24] who had showed by TG that oxygen uptake by the $LaMnO_3$ lattice is negligible below 700 °C. After the treatment the diffraction patterns changed significantly (Fig. 1) and became reproducible; simultaneously the room-temperature resistivity decreased to approximately half its previous value. The results did not change after extra annealing under the same conditions. Consequently, the oxygen content of the film reached an equilibrium with the oxygen atmosphere at 1 bar and 750 °C, which provides the same reference state for the different film compositions under investigation. Thus, we used such post-deposition annealing for all compositions prepared.

The δ values were not determined in our work. The correct oxygen stoichiometry determination for the $Ln_{1-x}M_xMnO_{3+\delta}$ films has not yet been described. Even in the case of the bulk materials there is a lack of data. Reasons for this include the absence of a definite reference state (three oxidation states of manganese, namely Mn^{4+}, Mn^{3+}, Mn^{2+}, occur in the material with the change of oxygen stoichiometry[24,25]), sample prehistory effects owing to cation disorder with a high density of vacancies in both A and B cation sublattices and an oxygen diffusion rate which is too slow to obtain reliable results for bulk samples at low temperature.

$LaMnO_{3+\delta}$ is capable of reduction with decreasing the oxygen partial pressure. According to ref. 26, at 900 °C and $pO_2 = 10^{-6}$ atm $La_{1-x}Sr_xMnO_{3+\delta}$ has $\delta \approx 0$ for $0 \leqslant x \leqslant 0.5$. At $pO_2 = 0.21$ atm, $\delta \approx 0.15$ was reported for $LaMnO_{3+\delta}$ at 730 °C[25] and $\delta \approx$ 0.14 at 1100 °C.[26] With increasing x the δ range between the oxygenated and reduced forms decreased and tended towards 0 for $x \geqslant 0.3$.[26] In fact, we have observed a less profound change of the XRD pattern after annealing an $La_{0.7}Sr_{0.3}MnO_{3+\delta}$ film as compared to $La_{0.85}Sr_{0.15}MnO_{3+\delta}$. Various $(La,Ln)_{0.7}M_{0.3}MnO_3$ samples prepared in ref. 10 showed $\delta \approx 0$ over a wide range of oxygen partial pressure. Thus, we can expect that after the annealing our thin films have nearly the same oxygen stoichiometry and this factor does not contribute to the differences in their properties. Consequently we omit δ in the compound formulae written below.

XRD characterization

XRD patterns of the annealed films are similar to those of a cubic lattice without any splitting of the solely observed (00l) or (hh0) reflections (in the pseudocubic system) or superstructural peaks. This does not mean that the perovskite film is necessarily cubic because of the film orientation. The XRD pattern of the oriented perovskite film does not provide unequivocal data on the lattice symmetry or a full set of lattice parameters. If the parameters calculated from the (00l) or (hh0) zones coincide, which was the case for our films, then we have an indication that the lattice is cubic. Apparent cubic lattice parameters a for the films are shown in Fig. 2, which reveals a nearly linear dependence on the average ionic radius, r_A. The dependence is not trivial, because variation of r_A results in tilting and rotation of the MnO_6 octahedra building a three-dimensional array rather than a simple contraction of bond distances, as shown for bulk samples.[10,12] For the range of r_A under consideration, orthorhombic or rhombohedral (at the lower temperature) phases in the bulk were described. A distortion of the array formed by MnO_6 octahedra breaks up

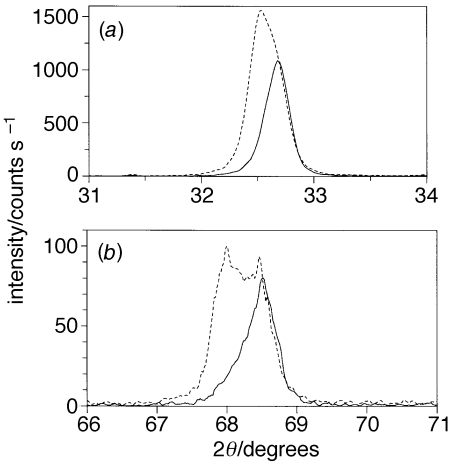

Fig. 1 Effect of subsequent annealing in oxygen at 750 °C for an $La_{0.85}Sr_{0.15}MnO_3$ film on YSZ: (*a*) (110) reflection, (*b*) (220) reflection. Dashed lines indicate the as-grown film, solid lines were obtained after annealing.

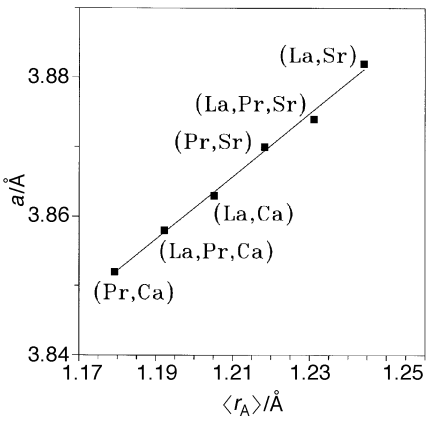

Fig. 2 Apparent lattice parameter, a, of $(La,Pr)_{0.7}(Sr,Ca)_{0.3}MnO_3$ perovskite films on MgO as a function of average ionic radius, $\langle r_A \rangle$, of the A site. The (002), (003), (110) and (220) peaks were used for the calculation. The a values found independently from (00l) and (hh0) peaks differ by less than 0.006 Å for all samples (Table 2).

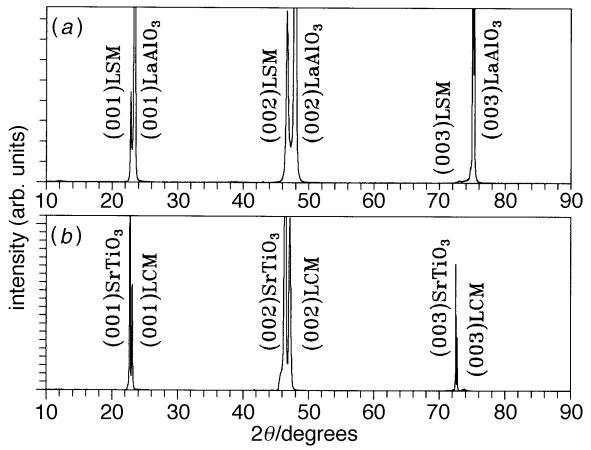

Fig. 3 Typical θ–2θ scans: (*a*) $La_{0.7}Sr_{0.3}MnO_3/LaAlO_3$, (*b*) $La_{0.7}Ca_{0.3}MnO_3/SrTiO_3$

the exchange of electrons governing magnetic properties and conductivity. Unfortunately, there is a lack of low-temperature XRD studies for the manganite thin films.

Perovskite substrates ($LaAlO_3$ $a=3.793$ Å, $SrTiO_3$ $a=3.905$ Å) permit the deposition of layers showing only (00*l*) reflections (Fig. 3); φ-scans prove the epitaxy of the 'cube-on-cube' type of deposition. Rocking curves measured for the (00*l*) reflections have FWHM = 0.17–0.25° [Fig. 4(*b*)], which indicates the high epitaxial quality of the films.

XRD patterns of $Ln_{1-x}M_xMnO_3/MgO$ reveal the (110) peak at thickness $d>2000$ Å. The large lattice mismatch between MgO ($a=4.21$ Å) and $Ln_{1-x}M_xMnO_3$ hinders the epitaxy of perovskites with $(001)_{film}\|(001)_{MgO}$. Deviation of the molar ratio Ln + M/Mn from unity results in the suppression of the (00*l*) orientation and the appearance of (*hh*0) peaks.

Analysis of the φ-scans shows that (00l)-oriented domains in the film on MgO have very good in-plane alignment: four-fold degeneracy of peaks is observed at a tilt angle equal to that between the plane under study and the (001) plane. Rocking curves for (00*l*) planes with FWHM $\approx 0.5°$ were measured for the best $Ln_{1-x}M_xMnO_3/MgO$ films [Fig. 4(*a*)].

$Ln_{1-x}M_xMnO_3$ on YSZ has a preferable orientation $(110)_f\|(001)_{YSZ}$. Even a pure $(110)_f\|(001)_{YSZ}$ orientation can be obtained for the manganites. The result correlates to the diagonal match with YSZ ($a\sqrt{3}$ to $5.14\times\sqrt{2}$). The FWHM of the rocking curves of the (220) reflection was 0.58° for $La_{0.7}Sr_{0.3}MnO_3$ on YSZ.

Surface morphology

Nearly stoichiometric films grow very smoothly up to until $d<2000$ Å. SEM images showed the featureless surface of such a film at a magnification of 5000–10000×. Small local disturbances were observed with increasing film thickness. In the range $d=2000$–3000 Å the surface changes from flat to hillocky. The hilliness becomes more marked for $d>3000$ Å, as was demonstrated also by AFM (Fig. 5). Such behaviour reflects the well known morphological instability of the CVD process controlled by diffusion in the gas phase.[27]

Deviation of the (Ln + M)/M ratio from the stoichiometric value in $Ln_{1-x}M_xMnO_3$ results in coarsening of the surface morphology even at a thickness $d\approx 1000$ Å.

Electrical properties

It was recently demonstrated for bulk samples[4,10,12] that for $La_{1-x}M_xMnO_3$ the P→FMM transition temperatures (both the resistivity maximum temperature, T_p, and the Curie temperature, T_c) can be presented in the form of a universal r_A dependence (certainly, at a constant Mn^{4+}/Mn^{3+} ratio). The

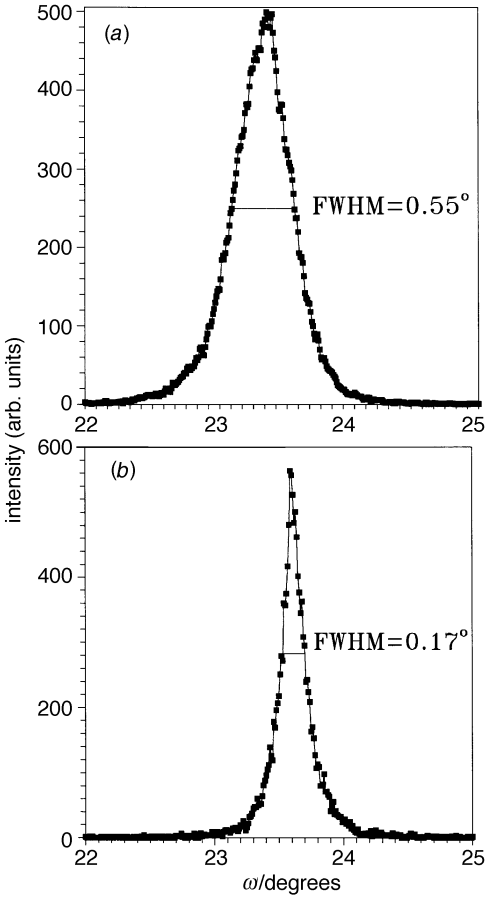

Fig. 4 Representative rocking curves for the (002) reflections of $(La_{1-x},Pr_x)_{0.7}M_{0.3}MnO_3$: (*a*) $La_{0.35}Pr_{0.35}Ca_{0.3}MnO_3/MgO$, (*b*) $La_{0.7}Ca_{0.3}MnO_3/SrTiO_3$

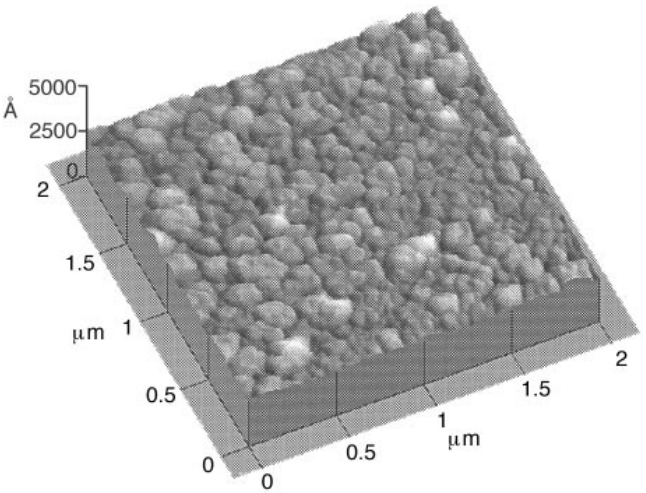

Fig. 5 AFM image of a 3500 Å thick $La_{0.7}Ca_{0.3}MnO_3$ film on $LaAlO_3$. The average roughness is 140 Å.

maximum T_p and T_c values, which exceed room temperature, conform to M = Sr at the optimal doping level $x=0.3$. Our data (Fig. 6) are in agreement with the prediction in ref 12. $La_{0.7}Sr_{0.3}MnO_3/LaAlO_3$ shows a metal-like temperature dependence of the resistivity in the range 77–300 K with a sharper increase of the resistivity as T approaches 300 K.

$La_{0.7}Ca_{0.3}MnO_3$ reveals a resistivity maximum at 230 K. This value practically coincides with the data for the bulk material of the same composition.[10] This value is also comparable with $T_p=220$ K for a $La_{0.72}Ca_{0.25}MnO_3/MgO$ thin film prepared by magnetron sputtering,[28] $T_p=250$ K for a

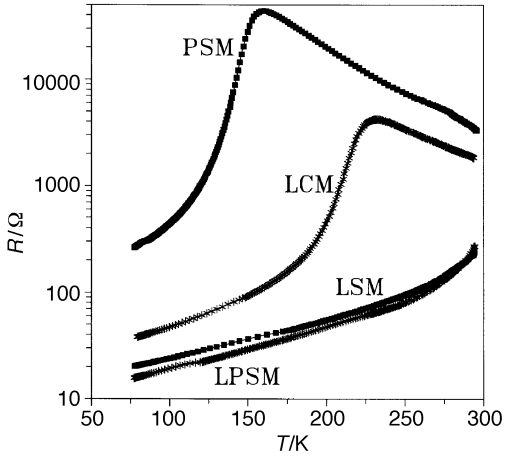

Fig. 6 Temperature dependence of the resistance of the films on $LaAlO_3$ (abbreviations are explained in Table 2)

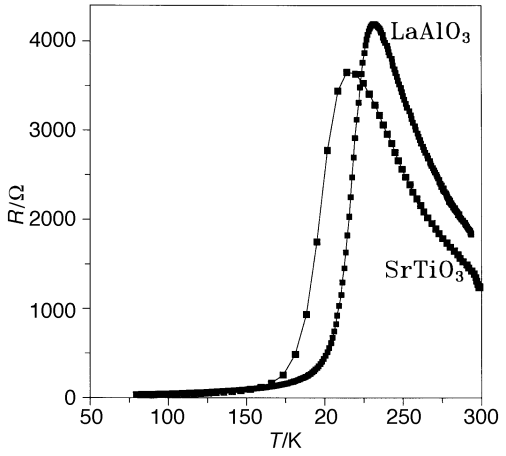

Fig. 7 Temperature dependence of the resistance of $La_{0.7}Ca_{0.3}MnO_3$ films on $LaAlO_3$ and $SrTiO_3$

$La_{0.67}Ca_{0.33}MnO_3/LaAlO_3$ thin film prepared by laser ablation and annealed in oxygen at 1000 °C,[29] $T_p = 270$ K for $La_{0.8}Ca_{0.2}MnO_3/LaAlO_3$ and $T_p = 245$–275 K for $La_{0.67}Ca_{0.33}MnO_3/LaAlO_3$ films prepared by MOCVD.[21,30]

On the other hand, T_p and T_c values for $La_{1-x}Ca_xMnO_3$ films prepared by laser ablation are known to be strongly influenced by variation of post-deposition annealing: for instance, $T_p \approx 95$ K and $T_p > 300$ K were reported for $La_{0.67}Ca_{0.33}MnO_3/LaAlO_3$.[19,29] One can suppose that variation of the Mn^{4+}/Mn^{3+} ratio occurs in such films owing to: (1) perhaps a broader δ range between the reduced and oxygenated states than that for $La_{1-x}Sr_xMnO_3$; (2) structural disorder induced in the film at the preparation stage; (3) deviations of cation stoichiometry, especially the La + Ca/Mn ratio. The exact reason for this variation is not yet known.

In ref. 19 it was suggested that epitaxial quality of the films is responsible for the shift of T_p. This suggestion seems rather unlikely, taking into account the proximity of T_p values listed above for ceramics and thin film materials prepared by different techniques, and the different epitaxial quality. Next, anomalous T_p were observed only for films as-grown under low pO_2 or after high-temperature (*ca.* 1000 °C) annealing in oxygen. In both cases variation of the Mn^{4+}/Mn^{3+} ratio is much more likely than a change of the epitaxial quality. It is worth mentioning that it is incorrect to assume that higher ρ means better epitaxy.[19] In fact, the metallic conductivity should be of the same order of magnitude for all compositions, but the resistivity of the P phase increases exponentially if this phase expands its stability field to lower temperature. Hence, $La_{1-x}Ba_xMnO_3$ or $La_{1-x}Sr_xMnO_3$ films can be of the same epitaxial quality as $La_{1-x}Ca_xMnO_3$ ones, but they still have higher T_p values.

Another remarkable feature of $La_{1-x}Ca_xMnO_3$ films was described in ref. 21. The T_p value was found to be dependent on the substrate material: an $La_{0.8}Ca_{0.2}MnO_3$ film on MgO has $T_p = 240$ K and a broader transition width than a film on $LaAlO_3$ ($T_p = 270$ K). The origin of the effect is not clearly understood yet: on the one hand, since the lattice mismatch between the film and the substrate has the opposite sign for $LaAlO_3$ and MgO and is significantly larger for MgO, strain can be induced in the film superimposing a deformation on the three-dimensional array of the MnO_6 octahedra, while on the other hand, since the film on MgO was not purely epitaxial [a low-intensity (110) reflection was observed in the XRD diffraction pattern[21]], the epitaxial quality could influence T_p.

In order to clarify this effect we compared $La_{0.7}Ca_{0.3}MnO_3$ films on $LaAlO_3$ and $SrTiO_3$. According to the XRD characterization both films were of the same epitaxial quality. Resistivity curves are very similar for both films (Fig. 7); after normalization to maximum resistivity they practically match each other after a 20 K shift along the temperature axis. Taking into account the lattice parameters of the substrates one can see that they possess nearly equal but opposite lattice mismatch with the film. Furthermore, according to ref. 21, T_p values of the epitaxial films on $LaAlO_3$ and $NdGaO_3$ [the latter has a very low lattice mismatch with the film (*ca.* 0.3%)] are very close. Thus, a tension but not a constriction of the film in the interface plane results in the change of T_p. An HREM study is desirable to understand which way the tension at the interface influences the properties of the whole film.

Along with variation of r_A by changing the M cation, one can also vary r_A value by changing Ln. Fig. 6 shows that in this case the electrical properties do not vary gradually with r_A. In fact, the resistivity curves for $La_{0.7}Sr_{0.3}MnO_3$ and $La_{0.35}Pr_{0.35}Sr_{0.3}MnO_3$ are similar, while $Pr_{0.7}Sr_{0.3}MnO_3$ reveals quite different behaviour. Certainly, T_p is expected to diminish with decreasing r_A, but gradually.[10,12]

As was mentioned in the introduction, the substitution of La for Pr or Nd leads to much more drastic changes in the electrical and magnetic properties than one would expect from the variation of r_A. Study of bulk materials points to the formation of charge- and spin-ordered phases.

Let us try to construct a conceptual phase diagram of $Ln_{1-x}M_xMnO_3$. Restricting the consideration by collinear spin ordering, we have ferromagnetic or antiferromagnetic states as well as a spin-disordered paramagnetic state. Superposition of the possible charge ordering (in other words, the ordered array of Mn^{4+} and Mn^{3+} ions[31]) and magnetic ordering increases the number of phase states by a factor of 2: $3 \times 2 = 6$ states. The relative positions of the phase fields in the coordinates temperature–magnetic field can be predicted in general: the paramagnetic phase occupies the whole high-temperature area, the antiferromagnetic state tends to low temperature and zero field, charge ordering is stabilized by decreasing temperature, and the ferromagnetic state is reinforced by the magnetic field. Less evident but proven[13,15] for $Ln_{1-x}M_xMnO_3$ is the fact that a magnetic field destroys charge-ordered states. These relationships are illustrated by Fig. 8 which turns out to be a good guide for comparing the properties of $Ln_{1-x}M_xMnO_3$. Depending on Ln and M, the position of the zero field line (or the T-axis) changes. In high field only FMM and P states are present. Thus, in high field, $Ln_{1-x}M_xMnO_3$ with small r_A would approximate the behaviour of $La_{1-x}Sr_xMnO_3$ in zero field. For instance, $Pr_{0.65}Ca_{0.35}MnO_3$ requires $H \approx 12$ T for such a transformation. Comparison of the $La_{1-x}Ca_xMnO_3$ and $Pr_{1-x}Ca_xMnO_3$ positions in the conceptual phase diagram leads to the idea that the solid solution of the phases will be subjected to such a transformation in lower field; in other

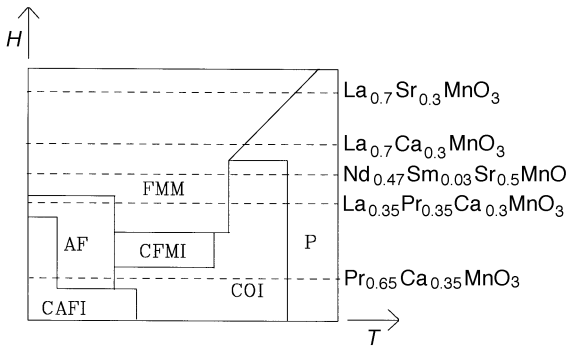

Fig. 8 Conceptual phase diagram of $Ln_{1-x}M_xMnO_3$: P, paramagnet; COI, charge-ordered state of paramagnet; FMM, ferromagnet with metal-like conductivity; CFMI, charge-ordered ferromagnet; AF, antiferromagnet; CAFI, charge-ordered antiferromagnet. Dashed line indicates the position of the *T*-axis (zero magnetic field) floating depending on Ln and M.

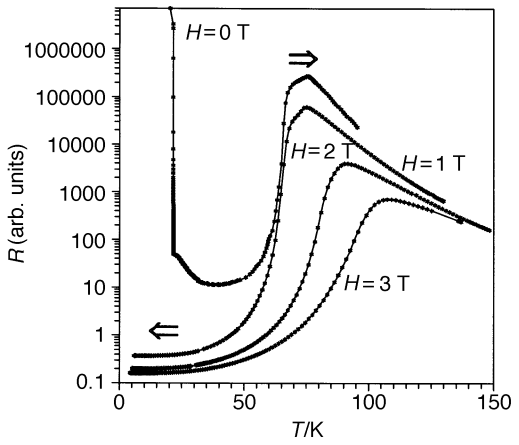

Fig. 9 Temperature dependence of the resistance of $La_{0.35}Pr_{0.35}Ca_{0.3}MnO_3/LaAlO_3$ for different magnetic field values

words, increasing r_A (up to that of $La_{1-x}Sr_xMnO_3$) and increasing the field have equivalent influences.

It is noteworthy that different phase fields in the diagram differ drastically in resistivity and its temperature dependence. High conductivity is possible only in the case of ferromagnetic ordering due to spin coupling of the itinerant (derived from e_g states) and localized (derived from t_{2g} states) electrons of Mn ions. If the atomic spins of the Mn ions are disordered or ordered antisymmetrically, then electronic exchange will be suppressed. In the case of antiferromagnetic order the resistivity should be higher than in the case of paramagnetic disorder, as between disordered atomic spins some nearly parallel spins occur, hence short-range exchange of electrons is possible. The antiparallel ordering of spins is accompanied by charge ordering in $Ln_{1-x}M_xMnO_3$,[13,15] in turn the charge-ordered phase derived from the paramagnetic state tends to result in an antiferromagnetic-like temperature dependence of the magnetization.[32] Thus, the phase transitions from these ordered states to the FMM state give rise to a drastic change of the resistivity. Being induced by a magnetic field, they produce ρ values much larger than those caused by the influence of the magnetic field on the FMM→P transition. Therefore, phases in which the zero field line intersects CAFI, AF or COI phase areas (Fig. 8), are expected to demonstrate very large ρ values in a moderate field. Such a situation occurs at about half height of the conceptual phase diagram.

This conclusion is well supported by experiments on $Nd_{0.47}Sm_{0.03}Sr_{0.5}MnO_3$,[32] $Pr_{0.7}Ca_{0.25}Sr_{0.05}MnO_3$ [11] and very recently $La_{1/3}Nd_{1/3}Ca_{1/3}MnO_3$.[33] Here we report a new example. A thin film of $La_{0.35}Pr_{0.35}Ca_{0.3}MnO_3$ on $LaAlO_3$ reveals a very complicated temperature dependence of the resistivity (Fig. 9). The magnetic measurements were not accomplished in the work; consequently the assignment of the magnetic states can be only preliminary and based on analogy.[13–15] The behaviour of the film resistivity was different depending on which process (cooling or heating) was used. Upon cooling the resistivity increased exponentially and became immeasurable below 70 K. After cooling to 4.2 K the specimen was heated, and it demonstrated a sharp drop of resistivity in the range 20–70 K (Fig. 9). Above 80 K the cooling and heating curves converged.

The hysteresis effects observed earlier[13–15] were explained by charge ordering of the P phase (probably overlapped by canted aniferromagnetism). As the result, the first-order phase transition FMM→COI takes place. For $Pr_{1-x}Ca_xMnO_3$ ($x \approx 0.3$–0.4) only the COI phase is stable in zero field. In a magnetic field of *ca.* 4–5 T at temperatures < 100 K the first-order phase transition was induced. At temperatures below 25–30 K the metastable FMM state could be frozen after removal of the field. In ref. 14 it was indirectly shown that ordering of Pr moments may be responsible for this effect.

The $La_{0.35}Pr_{0.35}Ca_{0.3}MnO_3/LaAlO_3$ specimen differs from $Pr_{1-x}Ca_xMnO_3$ in two important aspects: (1) the FMM phase formed spontaneously under heating is actually stable in the range 20–70 K; (2) the hysteresis takes place without an external magnetic field. The first distinction agrees with the conceptual phase diagram discussed above. The second distinction means that one more phase transition occurs at about 20 K in $La_{0.35}Pr_{0.35}Ca_{0.3}MnO_3/LaAlO_3$. By analogy with $Pr_{1-x}Ca_xMnO_3$ one can suppose the ordering of Pr moments, but spontaneously. Certainly, some other mechanism may be possible. At any rate, the phase transition can explain why heating after cooling to 4.2 K results in a low resistivity window at 20–70 K, but heating after cooling to 60 K does not (at 60 K resistivity tended to immeasurably large values).

In accordance with its expected position in the conceptual phase diagram, $La_{0.35}Pr_{0.35}Ca_{0.3}MnO_3/LaAlO_3$ turns out to be very sensitive to the magnetic field. In a magnetic field of 1 T the cooling and heating resistivity curves are very close. Only the FMM phase can be detected below 75 K in this field. As a result very large ρ values were found below 21 K as well as around 70 K. Increasing the field to 3 T results in a nearly saturated GMR effect (Fig. 10). The *R*–*H* hysteresis was studied at 75 K in more detail. Curves obtained by increasing and decreasing the field differ significantly, which is characteristic for the COI→FMM transition[15] and corresponds to crystallization and melting of the charge-ordered state. Note that the

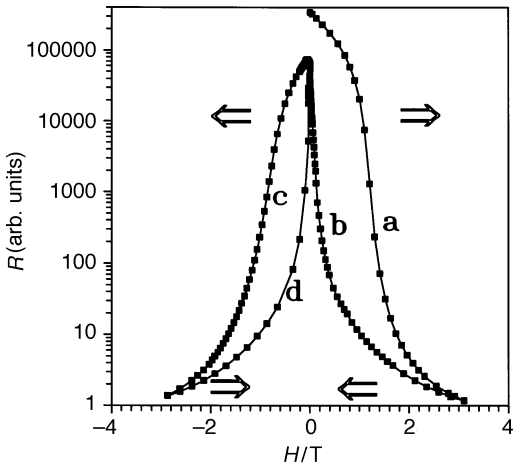

Fig. 10 Resistance, *R*, *vs.* magnetic field, *H*, loops for $La_{0.35}Pr_{0.35}Ca_{0.3}MnO_3/LaAlO_3$: the path direction is a-b-c-d

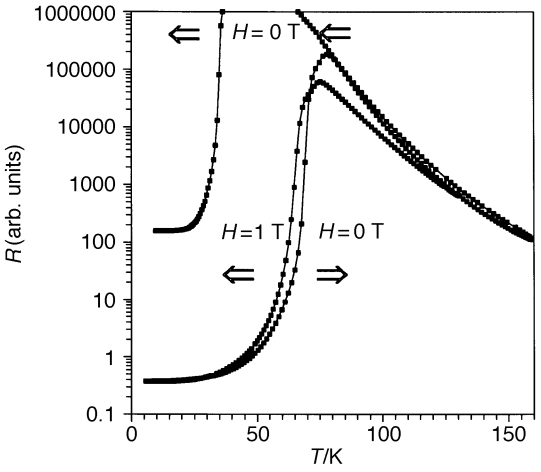

Fig. 11 Temperature dependence of the resistance of $La_{0.35}Pr_{0.35}Ca_{0.3}MnO_3/LaAlO_3$ cooled at $H=1$ T to 4.2 K with subsequent heating to 160 K and cooling in zero field

'crystallization' occurs in a very low field, *ca.* 0.2 T; nevertheless the resistivity in zero field was reproduced after cycling in a field of the opposite orientation. One can assume that careful variation of the temperature at about 70 K can provide an even lower saturation field as well as a thinner hysteresis loop, owing to the fact that the FMM phase is stable below 70 K.

It should be mentioned that the reproduced resistivity value in zero field after cycling in the magnetic field was several times lower than the initial zero field resistivity. This result may imply some remanent magnetization in the sample. An irreversible change of the magnetic state was assumed to be an alternative explanation in ref 14, where similar behaviour had been registered for $Pr_{0.6}Ca_{0.4}MnO_3$, but no remanent magnetization was detected by magnetic measurements.

Similar to $Pr_{1-x}Ca_xMnO_3$, the FMM state in $La_{0.35}Pr_{0.35}Ca_{0.3}MnO_3/LaAlO_3$ can be frozen in zero field after cooling in the magnetic field (even for $H=1$ T). Subsequent heating to 160 K in zero field produces a resistivity curve which looks like that one produced in a field (Fig. 11). The next cycle of cooling from 160 K leads to resistivity behaviour as described above for the sample which was not exposed to the magnetic field, except for in the low-temperature range. Below 35 K the resistivity drops again to a value about $10^3\times$ higher than the resistivity of the frozen FMM phase and was nearly constant below 20 K. This trend occurs for the subsequent heating too, but above 25 K the resistivity again approximates that of the sample not exposed to the field. It is noteworthy that $Pr_{0.6}Ca_{0.4}MnO_3$ reveals similar behaviour in a field of 4 T.[14] We see again, as for the sample not exposed to the magnetic field, that low-temperature reordering (probably with a contribution from Pr moments), which occurs in $Pr_{1-x}Ca_xMnO_3$ in the field, for $La_{0.35}Pr_{0.35}Ca_{0.3}MnO_3/LaAlO_3$ is spontaneous.

Conclusions

The results obtained by us and described in the literature for $Ln_{1-x}M_xMnO_3$ are in good agreement with the proposed conceptual phase diagram. There is an analogy between the magnetic field and r_A increase effects. Nevertheless the following specific points are worthy of note.

(a) If the ionic radii of cations in the A position vary significantly, then local stress may be important, which is the case for Ba-containing $Ln_{1-x}M_xMnO_3$. Next, the magnetic moment of rare-earth-metal cation cannot be neglected at low temperature.

(b) Antiferromagnetism and charge ordering were considered mainly independently in this study. Nevertheless the magnetic measurement data in the literature points to an interdependence of the phenomena.

(c) Non-collinear antiferromagnetism can be suspected in many particular cases.

At any rate, the idea that compositions most interesting for practical applications (owing to low saturation field, high ρ and $d\rho/dH$) should be searched at about the half-height level of the conceptual phase diagram, provides a good guide for further studies.

This research was partly supported by Volkswagen Foundation project I/69341 and RFBR grant no. 96–03–33027.

References

1 C. N. R. Rao and A. K. Cheetham, *Science*, 1996, **272**, 369.
2 M. H. Kryder, W. Messner and L. R. Cartley, *J. Appl. Phys.*, 1996, **79**, 4485.
3 T. Yotsuya, *Jpn. J. Appl. Phys.*, 1996, **35**, L23.
4 R. Mahesh, R. Mahendiran, A. K. Raychaudhuri and C. N. R. Rao, *J. Solid State Chem.*, 1995, **120**, 204.
5 R. von Helmolt, J. Wecker, B. Holzapfel, L. Shultz and K. Samwer, *Phys. Rev. Lett.*, 1993, **71**, 2331.
6 H. L. Ju, J. Gopalakrishnan, J. L. Peng, Q. Li, G. C. Xiong, T. Venkatesan and R. L. Greene, *Phys. Rev. B*, 1995, **51**, 6143.
7 R. Mahendiran, A. K. Raychaudhuri, A. Chainani, D. D. Sarma and S. B. Roy, *Appl. Phys. Lett.*, 1995, **66**, 233.
8 A. Urushibara, Y. Moritomo, T. Arima, A. Asamitsu, G. Kido and Y. Tokura, *Phys. Rev. B,* 1995, **51**, 14103.
9 P. Schiffer, A. P. Ramirez, W. Bao and S. W. Cheong, *Phys. Rev. Lett.*, 1995, **75**, 3336.
10 H. Y. Hwang, S. W. Cheong, P. G. Radaelli, M. Marezio and B. Batlogg, *Phys. Rev. Lett.*, 1995, **75**, 914.
11 B. Raveau, A. Maignan and V. Caignaert, *J. Solid State Chem.*, 1995, **117**, 424.
12 P. G. Radaelli, M. Marezio, H. Y. Hwang and S. W. Cheong, *J. Solid State Chem.*, 1996, **122**, 444.
13 Y. Tomioka, A. Asamitsu, Y. Moritomo, H. Kuwahara and Y. Tokura, *Phys. Rev. B*, 1996, **53**, 1689.
14 M. R. Lees, J. Barratt, G. Balakrishnan, D. McK. Paul and M. Yethiraj, *Phys. Rev. B*, 1995, **52**, 1.
15 H. Kuwahara, Y. Tomioka, A. Asamitsu, Y. Moritomo and Y. Tokura, *Science*, 1995, **270**, 961.
16 Y. Tomioka, A. Asamitsu, Y. Moritomo, H. Kuwahara and Y. Tokura, *Phys. Rev. Lett.*, 1995, **74**, 5108.
17 G. H. Jonker, *Physica*, 1956, **22**, 707.
18 G. C. Xiong, Q. Li, H. L. Ju, S. N. Mao, L. Senapati, X. X. Xi, R. L. Greene and T. Venkatesan, *Appl. Phys. Lett.*, 1995, **66**, 1427.
19 S. Jin, T. H. Tiefel, M. McCormack, R. A. Fastnacht, R. Ramesh and L. H. Chen, *Science*, 1994, **264**, 413.
20 K. Li, L. Liu, J. Sun, X. J. Xu, J. Fang, X. W. Cao, J. S. Zhu and Y. H. Zhang, *J. Phys. D*, 1996, **29**, 14.
21 Y. Q. Li, J. Zhang, S. Pombrik, S. DiMascio, W. Stevens, Y. F. Yan and N. P. Ong, *J. Mater. Res.*, 1995, **10**, 2166.
22 F. Weiss, K. Fröhlich, R. Haase, M. Labeau, D. Selbmann, J. P. Senateur and O. Thomas, *J. Phys., Colloq.*, 1993, **3**, 321.
23 O. Yu. Gorbenko, V. N. Fuflyigin, Y. Y. Erokhin, I. E. Graboy, A. R. Kaul, Yu. D. Tretyakov, G. Wahl and L. Klippe, *J. Mater. Chem.*, 1994, **4**, 1585.
24 J. A. M. van Roosmalen, P. van Vlaanderen, E. P. H. Cordfunke, W. L. Ijdo and D. J. W. Ijdo, *J. Solid State Chem.*, 1995, **114**, 516.
25 J. A. M. van Roosmalen and E. P. H.Cordfunke, *J. Solid State Chem.*, 1994, **110**, 109.
26 I. G. Krogh Andersen, E. Krogh Andersen, P. Norby and E. Skou, *J. Solid State Chem.*, 1994, **113**, 320.
27 C. H. J. Van den Brekel and A. K. Jansen, *J. Crystal Growth*, 1978, **43**, 364.
28 K. Chahara, T. Ohno, M. Kasai and Y. Kozono, *Appl. Phys. Lett.*, 1993, **63**, 1990.
29 M. Jaime, M. B. Salamon, K. Pettit, M. Rubinstein, R. E. Treece, J. S. Horwitz and D. B. Chrisey, *Appl. Phys. Lett.*, 1996, **68**, 1576.
30 G. J. Snyder, R. Hiskes, S. DiCarolis, M. R. Beasley and T. H. Geballe, *Phys. Rev. B*, 1996, **53**, 14434.
31 J. Goodenough, *Phys. Rev.*, 1955, **100**, 564.
32 H. Kuwahara, Y. Tomioka, Y. Moritomo, A. Asamitsu, M. Kasai, R. Kumai and Y. Tokura, *Science*, 1996, **272**, 80.
33 G. H. Rao, J. R. Sun, J. K. Liang, W. Y. Zhou and X. R. Cheng, *Appl. Phys. Lett.*, 1996, **69**, 424.

Paper 6/06465E; *Received* 19*th September*, 1996